JCTC Journal of Chemical Theory and Computation

Modeling Nitrogen Adsorption in Spherical Pores of Siliceous Materials by Density Functional Theory

E. A. Ustinov,[§] D. D. Do,*[,†] and M. Jaroniec[‡]

Department of Chemical Engineering, University of Queensland, St. Lucia, Queensland 4072, Australia, and Department of Chemistry, Kent State University, Kent, Ohio 44242

Received November 2, 2004

Abstract: Adsorption of nitrogen in spherical pores of FDU-1 silica at 77 K is considered by means of a nonlocal density functional theory (NLDFT) accounting for a disordered structure of pore walls. Pore size distribution analysis of various FDU-1 samples subject to different temperatures of calcination revealed three distinct groups of pores. The principal group of pores is identified as ordered spherical mesopores connected with each other by smaller interconnecting pores and irregular micropores present in the mesopore walls. To account for the entrances (connecting pores) into spherical mesopores, a concept of solid mass distribution with respect to the apparent density was introduced. It is shown that the introduction of the aforementioned distribution was sufficient to quantitatively describe experimental adsorption isotherms over the entire range of relative pressures spanning six decades.

1. Introduction

Over the past decades we have witnessed a markedly increasing interest in the analysis of adsorption phenomena in mesoporous materials. This was stimulated by discovery of highly ordered mesoporous materials such as MCM-41, SBA-15, SBA-16, and FDU-1 having cylindrical or spherical pores of controlled size. Adsorption isotherms for such adsorbents give scientists an opportunity to verify the capability of different theories to describe the hysteresis phenomena and properly characterize porous structure of solid materials. Analysis of adsorption in cylindrical pores is considered by means of continuum and molecular approaches. Examples of the former approaches are the Barret, Joyner, and Halenda (BJH) method,[1] the modified BJH method of Kruk, Jaroniec, and Sayari (KJS),[2] and the Broekhoff and de Boer (BdB) theory[3,4] and its many modified versions (modifications accounting for the solid−fluid potential dependence on the pore size,[5−7] dependence of the surface tension on the meniscus curvature,[8−12] and surface roughness[13]). Among molecular approaches applied for the analysis of adsorption in cylindrical pores the most frequently used are the nonlocal density functional theory (NLDFT)[14−22] and Monte Carlo technique.[17,23−25] The comparison of results obtained with the original BdB theory and the NLDFT[26] showed that they are close to each other for pores having a diameter greater than 7 nm. In general, the molecular approaches adequately represent features of adsorption in mesopores; however, some unresolved problems still remain. For example, the diameter of cylindrical pore determined with NLDFT is less than that determined with the X-ray diffraction technique (XRD) about 0.3−0.7 nm.[26] The lower closure point of the hysteresis is underestimated by the NLDFT (compared to 0.4 for nitrogen at 77 K and 0.34 for argon at 87.3 K[27] observed experimentally). The critical hysteresis diameter determined with the NLDFT for nitrogen adsorption at 77 K is 2 nm[15] (compared to 4 nm observed experimentally[28−30]). This difference is explained by the density fluctuations leading to nucleation via formation of bumps and bridges if the potential barrier is less than

* Corresponding author e-mail: duongd@cheque.uq.edu.au.
† University of Queensland.
‡ Kent State University.
§ On leave from Saint Petersburg State Technological Institute (Technical University), 26 Moskovsky Prospect, St. Petersburg 198013, Russia.

10.1021/ct049903z CCC: $30.25
Published on Web 05/04/2005

approximately 20 kT.[21,23,24,31] Another reason for an experimentally observed higher value of the critical hysteresis pore diameter could be energetic heterogeneity[32] or intrinsic pore size distribution.[33] Another unresolved issue is that which branch of the isotherm is equilibrium. According to the classical scenario of adsorption in cylindrical pores capillary evaporation occurs at equilibrium via receding menisci from the open ends of the pore, while the capillary condensation pressure corresponds to the limiting case of mechanical stability of metastable segment of adsorption branch of the isotherm (vaporlike spinodal point).[34] Nevertheless, some experimental investigations do not seem to support this scenario,[2,30,35−37] but instead they suggested that the adsorption branch of the isotherm corresponds to the true equilibrium. Our NLDFT analysis of condensation pressure for nitrogen and argon adsorption in MCM-41 samples in comparison with the XRD data also shows that the experimental condensation pressure−diameter dependence can be quantitatively matched only by the theoretical dependence obtained for the equilibrium transition pressure.[38]

Theoretical investigation of adsorption in spherical pores is very scarce in the literature. A comprehensive NLDFT analysis of nitrogen and argon adsorption in spherical pores of different siliceous adsorbents was recently presented by Ravikovitch et al.[21,39] The present paper is devoted to further development and refinement of the NLDFT method of analysis of adsorption isotherms in spherical pores. Our aim is to quantitatively describe nitrogen adsorption isotherms at 77 K in spherical pores of FDU-1 materials[40] over the entire range of relative pressures. We analyze a number of samples obtained at different temperatures of calcinations and derive their pore size distribution (PSD) functions. We proceed from the assumption that the average density of the solid constituting the pore wall is less than that for the reference nonporous silica due to the fraction of the surface of spherical pores is taken up by channels connecting spherical pores with each other. This average density is shown to be determined by the PSD analysis of the samples, which disclose important additional information on the pore structure of adsorbents.

2. Model

2.1. Nonlocal Density Functional Theory in the Case of Disordered Solids. In the present paper we use the Tarazona's smoothed density approximation[41,42] in our NLDFT formulation. The density distribution of a fluid confined in an open pore (grand canonical ensemble) corresponds to the minimum of the following grand thermodynamic potential

$$\Omega = \int \rho(\mathbf{r})[f(\mathbf{r}) - \mu]d\mathbf{r} \tag{1}$$

Here ρ is the local density in the pore; f is the molecular Helmholtz free energy; and μ is the chemical potential. The molecular Helmholtz free energy can be represented as a sum of four terms, representing the ideal, excess, attractive, and external part of the Helmholtz free energy, respectively

$$f(\mathbf{r}) = k_B T[\ln(\Lambda^3 \rho(\mathbf{r})) - 1] + f_{ex}[\bar{\rho}(\mathbf{r})] + u^{int}(\mathbf{r}) + u^{ext}(\mathbf{r}) \tag{2}$$

where Λ is the thermal de Broglie wavelength and k_B is the Boltzmann's constant. The excess Helmholtz free energy, $f_{ex}(\bar{\rho})$, accounts for the repulsive part of the interaction potential and is defined in the form of the Carnahan−Starling (CS) equation[43] derived for the equivalent hard sphere fluid:

$$f_{ex}(\bar{\rho}) = k_B T \frac{4\bar{\eta} - 3\bar{\eta}^2}{(1-\bar{\eta})^2},\ \bar{\eta} = \frac{\pi}{6} d_{HS}{}^3 \bar{\rho} \tag{3}$$

Here d_{HS} is the equivalent hard sphere diameter, and the smoothed density $\bar{\rho}$ is given by

$$\bar{\rho}(\mathbf{r}) = \int \rho(\mathbf{r}')\omega(|\mathbf{r} - \mathbf{r}'|;\bar{\rho}(\mathbf{r}))d\mathbf{r}' \tag{4}$$

The function $\omega(|\mathbf{r} - \mathbf{r}'|;\bar{\rho}(\mathbf{r}))$ in the integrand of the above equation is approximated by the following polynomial[42]

$$\bar{\rho}(\mathbf{r}) = \bar{\rho}_0(\mathbf{r}) + \bar{\rho}_1(\mathbf{r})\bar{\rho}(\mathbf{r}) + \bar{\rho}_2(\mathbf{r})(\bar{\rho}(\mathbf{r}))^2 \tag{5}$$

where

$$\bar{\rho}_i(\mathbf{r}) = \int \rho(\mathbf{r}')\omega_i(|\mathbf{r} - \mathbf{r}'|)d\mathbf{r}',\ i = 0,1,2 \tag{6}$$

The weight functions $\omega_0(r)$, $\omega_1(r)$, and $\omega_2(r)$ are defined as functions of the distance r in the region $0 < r < 2\ \sigma_{ff}$.[42] It is relevant to point here that the excess Helmholtz free energy may be interpreted as a function of the smoothed void volume $\bar{v} = 1 - \bar{\eta}$. The decrease of the void volume leads to the increase of repulsive forces. In the limiting case of zero value of the void volume there is no space to insert an additional molecule, which means infinite repulsive forces. This limiting case corresponds to the maximum possible value of the fluid density $\rho_m = 6/(\pi d_{HS}{}^3)$. The concept of the void volume is from a mathematical viewpoint exactly an equivalent way of the definition of the excess Helmholtz free energy of a homogeneous or inhomogeneous fluid far away from solid walls confining the fluid. However, the advantage of such a representation is that it accounts for the decrease in the void volume (that is the volume fraction available to fluid molecules) due to the increase in the fluid density as well as due to the presence of the solid wall. In this case repulsive forces acting between the wall and fluid molecules are also accounted for. The replacement of the density by the void volume allows us to consider the combined solid−fluid system from the same viewpoint as that developed for the inhomogeneous fluid. Such a consideration is justified for the case of amorphous solids because those could be treated as 'frozen' liquids and be a part of the system. This concept has been successfully applied to analysis of nitrogen and argon adsorption on nonporous silica[44] and in cylindrical pores of MCM-41 samples.[45,46] Below we briefly reproduce some basic points of this approach. Thus, in terms of void volume the excess Helmholtz free energy may be rewritten as follows:

$$f_{ex}(\bar{\rho}) = k_B T \frac{1 + 2\bar{v} - 3\bar{v}^2}{\bar{v}^2},\ \bar{v} = 1 - \bar{\rho}/\rho_m \tag{7}$$

In the above equation $\bar{v}$ is the smoothed void volume, which can be determined from the distribution of local void volume $v(\mathbf{r}) = 1 - \rho/\rho_m$ using the following equivalent form

of eqs 5 and 6

$$\bar{v}(\mathbf{r}) = \bar{v}_0(\mathbf{r}) + \rho_m \bar{v}_1(\mathbf{r})[1 - \bar{v}(\mathbf{r})] + \rho_m{}^2 \bar{v}_2(\mathbf{r})[1 - \bar{v}(\mathbf{r})]^2 \quad (8)$$

where

$$\bar{v}_i(\mathbf{r}) = \int v(\mathbf{r}')\omega_i(|\mathbf{r} - \mathbf{r}'|)d\mathbf{r}',\ i = 0,1,2 \quad (9)$$

The integration in the RHS of eq 9 has taken over the region of two fluid collision diameters. If the distance from the center of a given molecule to the pore wall surface is less than two collision diameters, the integral has taken over the space outside of the solid volume. It means that the local void volume inside the solid is zero, i.e., no one fluid molecule could reside inside the solid constituted the pore wall. Strictly speaking, such an assumption is not completely correct, as some molecules could penetrate to the solid and localize between solid atoms. Nevertheless, in the case of amorphous solids this assumption is more plausible compared to the formal application of the CS equation coupled with the Tarazona's prescription (5) and (6) to the solid−fluid interface. Indeed, in the latter case the local density of the fluid inside the solid is zero, which in accordance with eqs 3−6 is formally equivalent to the misleading statement that the void volume reaches maximum in the solid. In reality the replacement of the fluid molecules by the solid atoms never leads to the increase in the void volume (available to fluid molecules) up to its maximum value.

Contribution of the attractive potential to the Helmholtz free energy is usually modeled using the mean field approximation as follows:

$$u^{int}(\mathbf{r}) = \frac{1}{2}\int \rho(\mathbf{r}')\phi_{ff}(|\mathbf{r} - \mathbf{r}'|)d\mathbf{r}' \quad (10)$$

The pairwise potential ϕ_{ff} of two molecules is defined by the Weeks−Chandler−Andersen (WCA) scheme:[47]

$$\phi_{ff}(r) = \begin{bmatrix} -\epsilon_{ff} & r < r_m \\ 4\epsilon_{ff}[(\sigma_{ff}/r)^{12} - (\sigma_{ff}/r)^6] & r_m < r < r_c \\ 0 & r > r_c \end{bmatrix} \quad (11)$$

Here r and r_c are the distance between the molecules and the cutoff distance, respectively; ϵ_{ff} is the potential well depth; σ_{ff} is the collision diameter; $r_m = 2^{1/6}\,\sigma_{ff}$ is the distance at which the potential is minimum.

In the case of crystalline solids the external potential u^{ext} could be determined by integration of the 12-6 Lennard−Jones pairwise solid−fluid potential over the solid volume or surface, which for a flat interface results in the 9-3 or 10-4 potential, respectively. The resulting potential exerted by the solid has a form of the potential well, having minimum at a distance of about one solid−fluid collision diameter from the surface. The locus of the potential minimum is a two-dimensional plane parallel to the solid surface. Consequently, adsorption occurs as a sequential molecular layering, which is often reflected in highly undulated predicted adsorption isotherms, especially at low temperatures. In the case of disordered materials such as silica the centers of the outermost solid atoms are not located on a 2D surface. Therefore one could expect that the solid−fluid potential minimum is not as sharp as that observed with a crystalline surface but rather significantly dispersed. It is this dispersed minimum that prevents 2D condensation of the adsorbed fluid. There are approaches dealing with binary systems (so-called quenched−annealed (QA) systems), one part of which is a fluid (annealed) allowed to equilibrate, and the other one is the solid (quenched or frozen liquid).[48,49] Physical quantities of such systems are defined as double ensemble averages. The QA theory is quite involved. Therefore we apply an approach, which is simple in its description, but elegant enough to account for the dispersed minimum, and most importantly it is able to quantitatively describe nitrogen adsorption on amorphous surface of siliceous adsorbents.

Since repulsive forces arising between solid atoms and fluid molecules are already accounted for in the excess Helmholtz free energy using the concept of void volume, the only attractive term for the solid−fluid interaction is needed to be added. This could be done in a similar way used for the fluid−fluid interaction via the WCA perturbation scheme. For the system amorphous solid−fluid the WCA equation can be rewritten as follows

$$\phi_{sf}^{(j)}(r) = \begin{bmatrix} -\epsilon_{sf}^{(j)} & r < r_m^{(s)} \\ 4\epsilon_{sf}^{(j)}[(\sigma_{sf}/r)^{12} - (\sigma_{sf}/r)^6] & r_m^{(s)} < r < r_c^{(s)} \\ 0 & r > r_c^{(s)} \end{bmatrix} \quad (12)$$

where ϵ_{ff}, σ_{ff}, and $r_c^{(s)}$ are the solid−fluid potential well depth, the solid−fluid collision diameter, and the cutoff distance for the solid−fluid interaction, respectively. The superscript j at the pairwise potential and the potential well depth is 1 or 2 and is introduced to account for the distinction between atoms inside the solid ($j = 1$) and those on the solid surface ($j = 2$). It is important because in the general case the difference between the two can be very significant due to the surface functional groups such as silanols on the silica surface. Thus, the resulting external potential may be expressed as follows

$$u^{ext}(\mathbf{r}) = \int_V \rho_V^{(s)}\,\phi_{sf}^{(1)}(|\mathbf{r} - \mathbf{r}'|)d\mathbf{r}' + \int_S \rho_S^{(s)}\,\phi_{sf}^{(2)}(|\mathbf{r} - \mathbf{r}'|)d\mathbf{r}' \quad (13)$$

where $\rho_V^{(s)}$ and $\rho_S^{(s)}$ are the solid and surface density, respectively. The corresponding integrals are taken over the solid volume and surface.

2.1.1. Henry Law Limit. There could be a question as to whether the method of application of NLDFT to amorphous solids leads to the Henry law at low densities. At the limiting case of zero loading the fluid−fluid interaction potential vanishes. In this case the minimization of the grand thermodynamic potential leads to the following equation

$$k_B T \ln[\Lambda^3 \rho(\mathbf{r})] + f_{ex}[\bar{v}(\mathbf{r})] + u^{ext}(\mathbf{r}) = \mu \quad (14)$$

At negligibly small bulk pressure p and, as a consequence, the adsorbed fluid density and the smoothed void volume are a function of only the distance from the surface, and the chemical potential is proportional to $k_B T \ln p$. It means that

Table 1. Molecular Parameters for the System N_2 − Silica at 77 K

fluid − fluid			solid − fluid			
σ_{ff} (nm)	ϵ_{ff}/k_B (K)	d_{HS} (nm)	σ_{sf} (nm)	$\rho_V^{(s)}\,\epsilon_{sf}^{(1)}/k_B$ (K nm^{-3})	$\rho_S^{(s)}\,\epsilon_{sf}^{(2)}/k_B$ (K nm^{-2})	$r_c^{(s)}/\sigma_{sf}$
0.3575	94.45	0.3575	0.2988	6406	640.1	4.4

the fluid density is proportional to the bulk pressure at a specified point of space near the surface:

$$\rho(\mathbf{r}) = \frac{p}{k_B T} \exp\left[-\frac{f_{ex}[\bar{v}(\mathbf{r})] + u^{ext}(\mathbf{r})}{k_B T}\right] \qquad (15)$$

The proportionality between the density and the pressure results in linear dependence of the amount adsorbed on the bulk pressure, i.e., the adsorption isotherm reduces to the Henry law at a sufficiently low-pressure region, which confirms the correctness of the method under consideration. Our observation is that the Henry law region in the case of amorphous solids corresponds to much lower pressures compared to that for the conventional NLDFT. Some additional features of the adsorption isotherm on a nonporous amorphous solid under the monolayer coverage will be discussed in the next subsection.

It should be noted that the proposed approach is an extension of the conventional NLDFT to a binary system of fluid−amorphous solid, rather than its alternative. The reason this method as applied to amorphous solids works much better than the formal application of NLDFT to crystalline surfaces (it is shown below) is apparently associated with a smoother repulsive term of the solid−fluid potential due to random dispersion of solid atoms relative to the surface, which prevents artificial layering of the adsorbed fluid. Viewing fluid−fluid and fluid−solid interactions from the same standpoint seems to be justified in the case of amorphous solids despite some simplifications such as the neglect of the nonzero transition zone at the surface, thermodynamic inertness of the solid (the excess free energy of solid atoms in the vicinity of the surface is assumed to not be affected by the fluid molecules), and impermeability of the solid to fluid molecules. A more rigorous approach requires further investigations.

2.2. Adsorption on Nonporous Reference Material. The fluid−fluid molecular parameters are determined from the bulk properties (the saturation pressure and the liquid density at the saturation pressure) and surface tension. These parameters were taken from the paper of Neimark et al.[50] The solid−fluid parameters were determined by the least squares procedure from the nitrogen adsorption isotherm on nonporous silica LiChrospher Si-1000 at 77 K.[51] All molecular parameters are listed in Table 1.

Nitrogen adsorption isotherm on nonporous silica is presented in Figure 1 in logarithmic and linear scales. The solid line is plotted with the described above method of application of NLDFT to disordered solids using the parameters listed in Table 1. As one can see from the figure, the experimental isotherm is excellently fitted by the theoretical curve over the entire relative pressure range by six decades, which confirms the adequacy of the NLDFT approach. For comparison the dashed line in the figure shows the result of conventional NLDFT application, in which the solid is not a part of the binary solid−fluid system and is considered solely as a source of the external 10-4 LJ potential. The dashed line is calculated for the solid−fluid parameters presented in refs 18, 20, and 50. The Henry law region corresponding to our approach is not seen in Figure 1, but it exists in the lower pressure range. Interestingly, according to experimental data and the developed version of NLDFT there is a broad region between the Henry law and the monolayer coverage where the amount adsorbed increases gradually with pressure. This indirectly points to the energetic heterogeneity of silica surface, which formally could be described in the framework of the Langmuir model of adsorption on isolated sites distributed over their energy. It means that the proposed algorithm of NLDFT application to the amorphous surface implicitly accounts for its energetic heterogeneity at the microscopic level (as opposed to the patchwise model having macroscopic origin) caused by random spatial distribution of solid atoms in the vicinity of the surface.

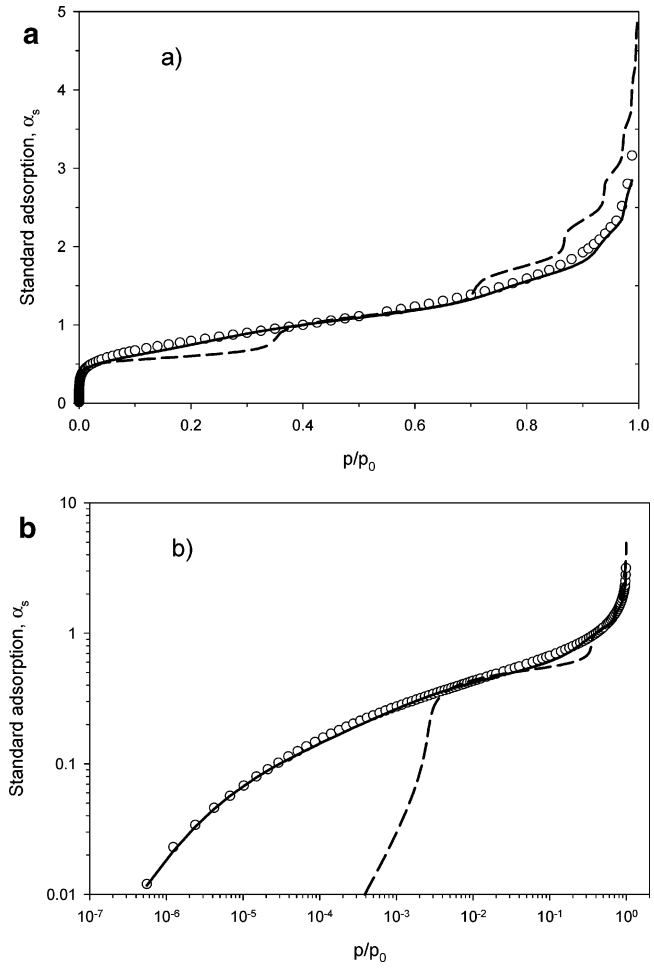

Figure 1. Nitrogen standard reduced adsorption isotherm on silica LiChrospher Si-1000 at 77.3 K in linear scale (a) and logarithmic scale (b). (Circles) experimental data,[51] (solid line) the developed version of NLDFT for amorphous surface, and (dashed line) conventional NLDFT with molecular parameters listed in Table 1.

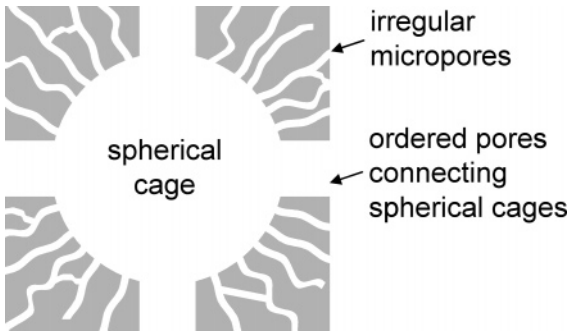

Figure 2. Illustration of a spherical cage with neighboring connecting pores and irregular micropores. Spherical cages together with connecting pores form a three-dimensional system of ordered mesopores, which in the case of FDU-1 has *Fm*3*m* symmetry.

2.3. Application of the NLDFT to Spherical Pores. In the present paper we considered a spherically symmetrical density distribution inside a spherical pore. This is a quite strong assumption since each spherical mesopore of FDU-1 silica has 12 windows connecting this pore with the neighboring pores. The two-dimensional diagram of a spherical pore with connecting channels as well as micropores is shown in Figure 2. The rigorous way is to solve the 3D task; however, this task is highly time-consuming, so the 1D spherically symmetrical model seems to be a reasonable simplification. In this 1D representation, the spherical pore is modeled as one without any connecting pores, and therefore the average density of solid atoms of this model pore would be less than the solid skeleton density of a real pore. We shall denote hereafter this average density as the apparent density. Since we do not exactly know the shape and volume of the connecting pores it makes sense to consider the average pore wall density as an adjustable parameter. The spherical pore volume was divided into the set of concentric spheres having radii incremented by 1/30 fluid−fluid collision diameter. For each pair of spherical surfaces the Tarazona's weight function and the WCA attractive potential were determined. Minimization of the functional (1) results in the set of equations relative to the set of local densities defined at the spherical surfaces at a given chemical potential. This set of equations is solved by a standard iteration procedure producing a density profile corresponding to the thermodynamic equilibrium. Having determined the density profile, one can easily calculate the apparent density at a given bulk phase pressure. In doing so, we determined a set of local isotherms for a set of pore size ranging from 0.72 to 21 nm at a specified apparent density of the pore wall. Note that the capillary rise that we refer to is the equilibrium transition pressure, rather than the vaporlike spinodal pressure. Besides we generated 60 sets of local isotherms, each of which corresponds to a specified pore wall density in the region from 0.88 to 2.2 g/cm^3.

We applied the NLDFT extended to amorphous solids to the adsorption branch of isotherms assuming that like in the case of cylindrical pores the adsorption branch for spherical pores is close to the true equilibrium.[36−38] Besides the pore size distribution the distribution function of mass of adsorbent with respect to the average pore wall density (MDF) was introduced in the following form

$$\xi(\rho_V^{(s)}) = \frac{d(m/m_0)}{d\rho_V^{(s)}} \tag{16}$$

where m/m_0 is the fraction of mass of adsorbent having apparent density of the pore wall less than $\rho_V^{(s)}$ and m_0 is the total mass of the sample. Note that the function ξ is normalized. For the sake of simplicity we assume that $\rho_S^{(s)}/\rho_V^{(s)}$ is constant. With the above definition the amount adsorbed can be expressed as follows:

$$a(p/p_0) = \int\int f(D)\xi(\rho_V^{(s)})\rho^a(p/p_0,D,\rho_V^{(s)})d(\rho_V^{(s)})d\log D \tag{17}$$

Here ρ^a is the density of adsorbed fluid at a relative pressure p/p_0 in the pore having diameter D and average pore wall density $\rho_V^{(s)}$; $f(D)$ is the pore size distribution function, that is

$$f(D) = \frac{dV}{d\log D} \tag{18}$$

The PSD and MDF were determined using the Tikhonov regularization method.[52,53] Details of application of the regularization method can be found elsewhere.[54,55]

3. Results

In the present paper we analyze nitrogen adsorption isotherms for a series of ordered mesoporous silica samples, FDU-1, having a cagelike structure.[40] Adsorption branches of isotherms for five samples calcined at different temperatures are presented in Figure 3. Pore size distribution functions determined for these isotherms are shown in Figure 4 in logarithmic and linear scales. It is seen from the figure that there are three distinct peaks in the PSDs. The first one in the region of equivalent spherical pore diameters from 0.8 to approximately 1.3 nm is associated with micropores in the pore walls. The second peak in the pore size region from 1.3 to 3 nm may be attributed to connecting pores between neighboring larger spherical pores, which are represented by the third peak in the PSD. The increase of the temperature of calcination leads to a decrease in the pore volume of all groups of pores as well as their sizes due to the shrinkage of the silica framework. In the case of micropores their average size does not change much because calcination may cause elimination of fine micropores[56] and/or substantial reduction of their size, making them inaccessible for adsorbate molecules.

Figure 5 shows the distribution of mass of the adsorbent with respect to the average pore wall density. The mass distribution functions (MDF) can be interpreted by considering the hypothetical case of ordered adsorbent having spherical pores of equal size connected with each other by channels whose surfaces are treated as hard walls (i.e., adsorption does not occur). With this hypothetical case, its MDF is a Dirac delta function at a density of the solid, and this density is less than the density of nonporous silica (2.2 g/cm^3). This is because the pore wall of the spherical pores is not continuum due to hollows, occupied by the connecting channels. Since the model considers the pore surface as a

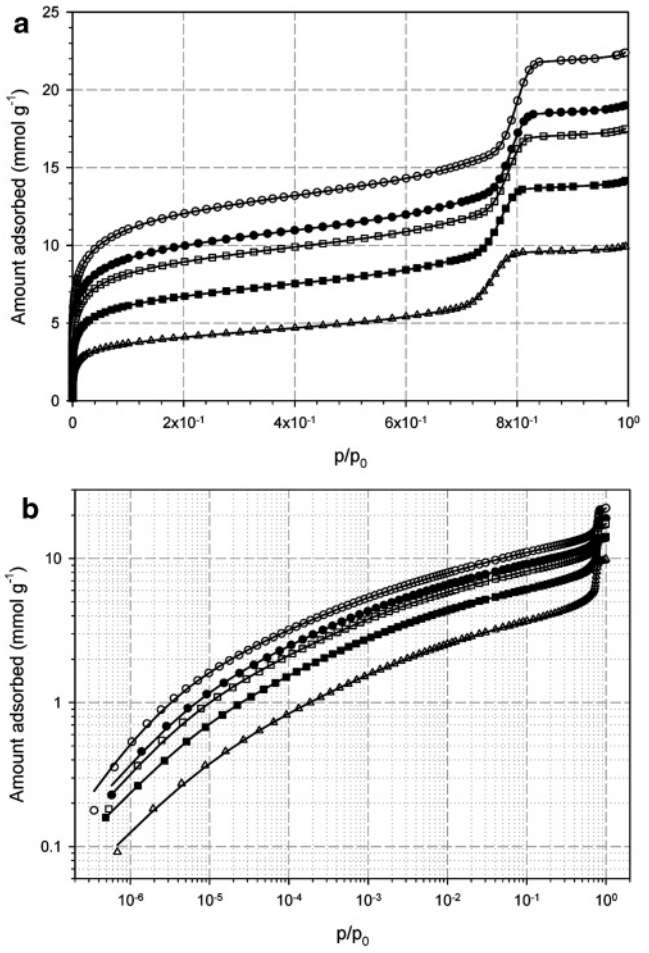

Figure 3. Nitrogen adsorption isotherm for FDU-1 samples at 77 K at linear scale (a) and in logarithmic scale (b). Temperature of calcinations (K): ○ − 813, ● − 973, □ − 1073, ■ − 1173, △ − 1273. Solid lines are correlated by the NLDFT version for amorphous solids.

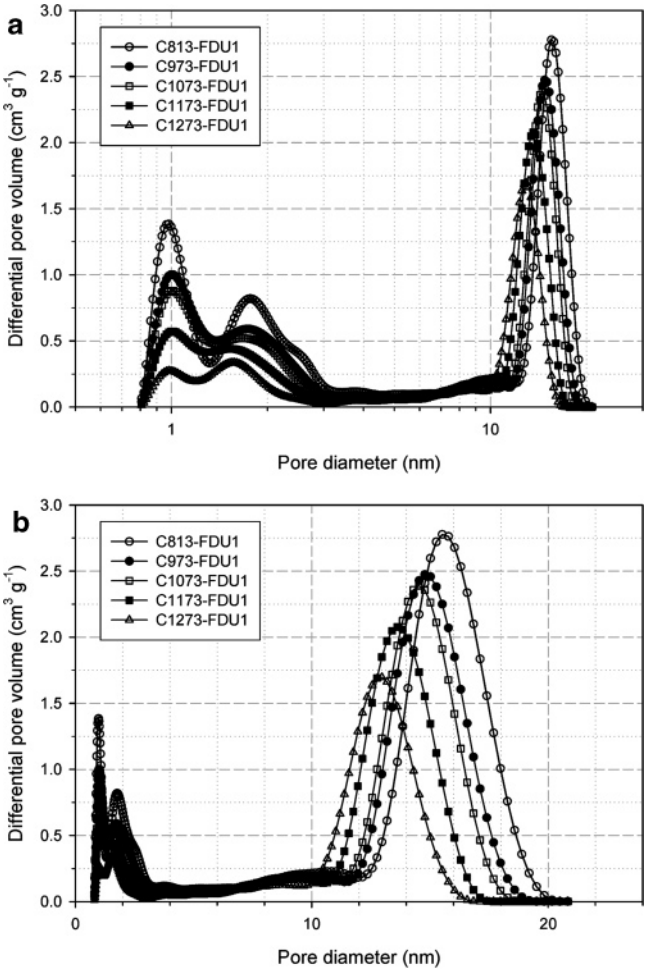

Figure 4. Pore size distributions for FDU-1 samples calcined at different temperature in logarithmic (a) and linear (b) scale obtained with the developed NLDFT version for amorphous solids. Three peaks from left to right correspond to micropores in pore walls, connecting pores, and spherical mesopores, respectively.

contiguous spherical wall, the apparent density of the solid constituting the wall must be decreased. Now let the connecting channels be adsorbing pores. In this case we have to account for two kinds of pores (main spherical mesopores and connecting pores) having a different size and, most importantly, a different apparent density of the pore walls. The latter is due to the different geometry of those pores and numbers of windows. It leads us to the conclusion that the MDF should consist of at least two peaks. This is exactly what we observe on the MDF in Figure 5. However, any further geometrical considerations should be done with reservations for the following reasons. First, the model is one-dimensional, while the pore has a number of hollows, which destroys the spherical symmetry. Second, little is known about the geometry of connecting pores, though we model them as spherical pores (as well as micropores) the same way as we do for the main pores. Third, the PSD function and MDF are uncorrelated, which is generally not correct. Any attempts to correlate these are bound to great complication, due to the ill-posed nature of the task under consideration. It is interesting to note that the MDF is nearly the same for all samples despite the significant decrease in the pore volume with the temperature of calcination. It could be explained by a proportional shrinkage of solid and pore volume, which keeps unchanged the relation between pore size and windows for each group of pores. There is some uncertainty about which peak corresponds to larger spherical pores and that to connecting pores, but it is likely that the average pore wall density for the main spherical pores is about 0.75 $\rho_{V0}^{(s)}$, i.e., 1.65 g/cm^3 since the right peak is larger compared to the left one, which is in agreement with the PSD functions.

All characteristics of the porous structure of analyzed samples are summarized in Table 2.

The subscripts 'me', 'con', and 'mi' denote (spherical) mesopores, connecting pores, and micropores, respectively. Corresponding volumes were determined by integration of the PSD function in the regions of size 10−21, 1.3−3, and 0.8−1.3 nm, respectively. The pore diameters were determined using the maximum of the corresponding peak. The surface area is determined only for the main spherical pores, S_{me}, as the physical shape of micropores and connecting pores is not known exactly. Besides, we also determined the external surface S_{ex}, whose contribution to the amount adsorbed was accounted for by using the *t*-curve for nitrogen

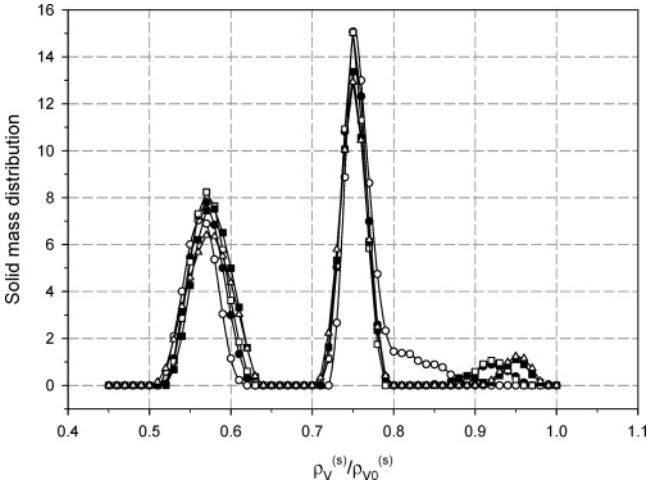

Figure 5. Mass distribution of silica $\rho_{V0}^{(s)}\xi(\rho_V^{(s)})$ with respect to the average pore wall density for series of FDU1 silica samples calcined at different temperatures (K): ○ − 813, ● − 973, □ − 1073, ■ − 1173, △ − 1273. $\rho_{V0}^{(s)}$ is the density of continuous nonporous silica (2.2 g/cm^3). The area under each curve is unity.

Table 2. Structural Parameters for the Series of FDU1 Samples

sample	D_{me} (nm)	D_{con} (nm)	D_{mi} (nm)	V_{me} (nm)	V_{con} (nm)	V_{mi} (nm)	S_{me} (m^2/g)	S_{ex} (m^2/g)
C-813	15.5	1.77	0.98	0.31	0.19	0.18	124	12
C-973	14.8	1.74	1.00	0.27	0.15	0.15	112	11
C-1073	14.5	1.68	1.00	0.26	0.13	0.13	108	10
C-1173	13.6	1.53	1.01	0.22	0.10	0.09	100	10
C-1273	13.0	1.55	0.99	0.18	0.06	0.04	86	7

adsorption on nonporous silica LiChrospher Si-1000.[51] Analysis of the data presented in Table 2 shows that the increase of the temperature of calcination decreases the size of spherical mesopores and connecting pores but does not affect the size of micropores. The surface of mesopores and their diameter both decrease with the increase of calcination temperature. It raises the question whether the number of (available) pores is affected by the temperature. Figure 6 gives one more piece of information on this matter. In this figure we present the distribution function of number of pores with respect to the pore size defined as

$$\varphi(D) = \left(\frac{\pi D^3}{6}\right)^{-1} \frac{dV}{d\log D} \tag{19}$$

Figure 6a shows the distribution in the whole region of pore size. Due to the relatively small size of micropores their number is very large compared to mesopores, so the distribution function in the region above 2 nm is not seen. One can see from the figure that the increase of the calcination temperature does not change the pore size of micropores but substantially decreases their number. It could mean that calcination leads to progressive blocking of micropores and/or their elimination.[56] The situation is different if this figure is plotted in a small scale for the region of pores larger than 5 nm (Figure 6b). It is seen from the figure that all distribution functions related to the main

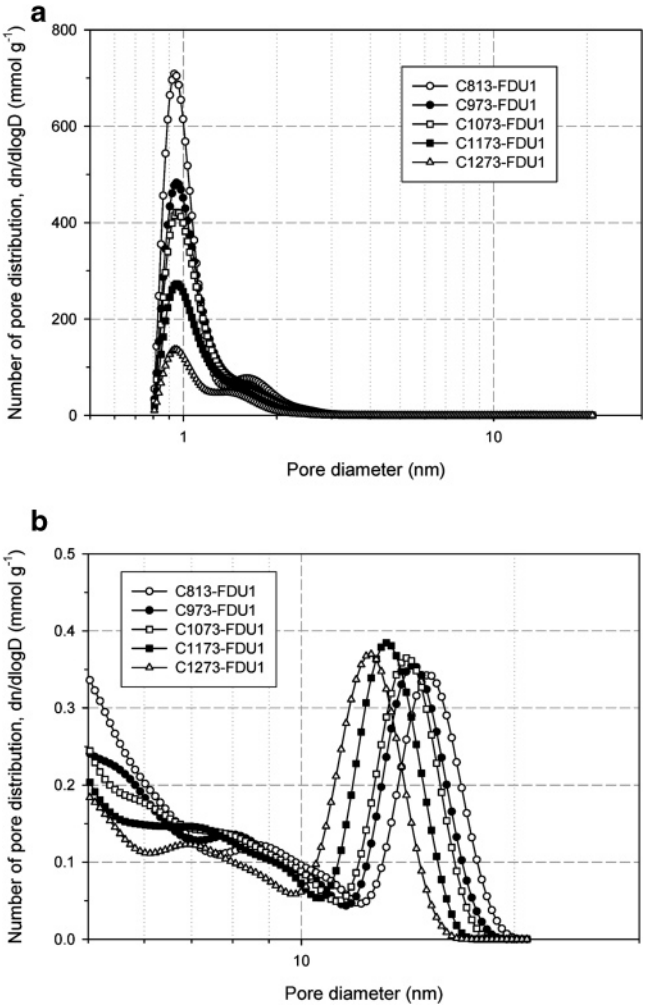

Figure 6. Distribution of number of pores of FDU-1 samples calcined at different temperatures: (a) the whole region of pores and (b) the region of spherical mesopores.

spherical mesopores are nearly the same, but the increase of the temperature of calcination just shifts them toward smaller pore size. It confirms the conclusion that geometrical mesopore structure remains the same during calcination, but the pore size and the pore wall thickness decrease in the same proportion, i.e., the adsorbent shrinks isotropically. The external surface, as is seen from Table 2, also decreases with the increase of the temperature.

4. Conclusion

The nonlocal density functional theory extended for the case of amorphous surfaces is presented. We demonstrated results of the application of the new version of NLDFT to spherical pores of a series of silica FDU-1 samples obtained with a progressive increase in the temperature of calcination. The model quantitatively describes nitrogen adsorption isotherms at 77 K over the entire pressure range. It was found that the apparent density of the pore wall is smaller than that for the nonporous silica due to intermediate pores connecting spherical mesopores. The increase of the calcination temperature leads to blocking micropores and shrinkage of mesopores; however, the geometrical structure of the adsorbent remains the same. The proposed model and method

of simultaneous pore size and mass distribution analysis is a convenient tool for characterization of amorphous porous solids.

Acknowledgment. Support from the Australian Research Council is gratefully acknowledged. M.J. acknowledges NSF for a partial support of this research (grant CHE-0093707).

References

(1) Barrett, E. P.; Joyner, L. G.; Halenda, P. P. *J. Am. Chem. Soc.* **1951**, *73*, 373−380.

(2) Kruk, M.; Jaroniec, M.; Sayari, A. *Langmuir* **1997**, *13*, 6267−6273.

(3) Broekhoff, J. C. P.; de Boer, J. H. *J. Catal.* **1967**, *9*, 8−14, 15−27.

(4) Broekhoff, J. C. P.; de Boer, J. H. *J. Catal.* **1968**, *10*, 368−376, 377−390, 391−400.

(5) Zhu, H. Y.; Lu, G. Q.; Zhao, X. S. *J. Phys. Chem. B* **1998**, *102*, 7371−7376.

(6) Qiao, S. Z.; Bhatia, S. K.; Zhao, X. S. *Microporous Mesoporous Mater.* **2003**, *65*, 287−298.

(7) Qiao, S. Z.; Bhatia, S. K.; Nicholson, D. *Langmuir* **2004**, *20*, 389−395.

(8) Sonwane, C. G.; Bhatia, S. K. *Chem. Eng. Sci.* **1998**, *53*, 3143−3156.

(9) Bhatia, S. K.; Sonwane, C. G. *Langmuir* **1998**, *14*, 1521−1524.

(10) Sonwane, C. G.; Bhatia, S. K. *Langmuir* **1999**, *15*, 5347−5354.

(11) Sonwane, C. G.; Bhatia, S. K.; Calos, N. *Ind. Eng. Chem. Res.* **1998**, *37*, 2271−2283.

(12) Sonwane, C. G.; Bhatia, S. K. *J. Phys. Chem. B* **2000**, *104*, 9099−9110.

(13) Inoue, S.; Hanzawa, Y.; Kaneko, K. *Langmuir* **1998**, *14*, 3079−3081.

(14) Ravikovitch, P.; Domhnaill, S.; Neimark, A.; Schuth, F.; Unger, K. *Langmuir* **1995**, *11*, 4765−4772.

(15) Ravikovitch, P. I.; Wei, D.; Chueh, W. T.; Haller, G. L.; Neimark, A. V. *J. Phys. Chem. B* **1997**, *101*, 3671−3679.

(16) Ravikovitch, P. I.; Neimark, A. V. *Stud. Surf. Sci., Catal.* **2000**, *129*, 597−606.

(17) Neimark, A. V.; Ravikovitch, P. I.; Vishnyakov, A. *Phys. Rev. E* **2000**, *62*, 1493−1496.

(18) Ravikovitch, P. I.; Vishnyakov, A.; Neimark, A. V. *Phys. Rev. E* **2001**, *64*, 011602/1−011602/20.

(19) Ravikovitch, P. I.; Neimark, A. V. *Colloids Surf., A* **2001**, *187−188*, 11−21.

(20) Neimark, A. V.; Ravikovitch, P. I. *Microporous Mesoporous Mater.* **2001**, *44−45*, 697−707.

(21) Ravikovitch, P. I.; Neimark, A. V. *Langmuir* **2002**, *18*, 9830−9837.

(22) Cao, D.; Shen, Z.; Chen, J.; Zhang, X. *Microporous Mesoporous Mater.* **2004**, *67*, 159−166.

(23) Gelb, L. D. *Mol. Phys.* **2002**, *100*, 2049−2057.

(24) Vishnyakov, A.; Neimark, A. V. *J. Chem. Phys.* **2003**, *119*, 9755−9764.

(25) Coasne, B.; Pellenq, R. J.-M. *J. Chem. Phys.* **2004**, *120*, 2913−2922.

(26) Neimark, A. V.; Ravikovitch, P. I.; Vishnyakov, A. *J. Phys.: Condens. Matter* **2003**, *15*, 347−365.

(27) Kruk, M.; Jaroniec, M. *Chem. Mater.* **2001**, *13*, 3169−3183.

(28) Kruk, M.; Jaroniec, M.; Sayari, A. *J. Phys. Chem. B* **1997**, *101*, 583−589.

(29) Franke, O.; Schulz-Ekloff, G.; Rathousky, J.; Starek, J.; Zukal, A. *J. Chem. Soc., Chem. Commun.* **1993**, 724−726.

(30) Branton, P. J.; Hall, P. G.; Sing, K. S. W. *J. Chem. Soc., Chem. Commun.* **1993**, 1257−1258.

(31) Vishnyakov, A.; Neimark, A. V. *J. Phys. Chem. B* **2001**, *105*, 7009−7020.

(32) Maddox, M. W.; Olivier, J. P.; Gubbins, K. E. *Langmuir* **1997**, *13*, 1737−1735.

(33) Kruk, M.; Jaroniec, M.; Sayari, A. *Adsorption* **2000**, *6*, 47−51.

(34) Everett, D. H. In *The Solid−Gas Interface*; Flood, E. A., Ed.; Marcel Dekker: New York, 1967; Vol. 2, Chapter 36, p 1055.

(35) Kruk, M.; Jaroniec, M. *J. Phys. Chem. B* **2002**, *106*, 4732−4739.

(36) Morishige, K.; Ito, M. *J. Chem. Phys.* **2002**, *117*, 8036−8041.

(37) Morishige, K.; Nakamura, Y. *Langmuir* **2004**, *20*, 4503−4506.

(38) Ustinov, E. A.; Do, D. D. Capillary phenomena in the framework of the two-dimensional density functional theory. *Fundamentals of Adsorption 8.* Sedona, Arizona, U.S.A. May 23−28 2004.

(39) Ravikovitch, P. I.; Neimark, A. V. *Langmuir* **2002**, *18*, 1550−1560.

(40) Kruk, M.; Celer, E. B.; Jaroniec, M. *Chem. Mater.* **2004**, *16*, 698−707.

(41) Tarazona, P. *Phys. Rev. A* **1985**, *31*, 2672−2679.

(42) Tarazona, P.; Marconi, U. M. B.; Evans, R. *Mol. Phys.* **1987**, *60*, 573−595.

(43) Carnahan, N. F.; Starling, K. E. *J. Chem. Phys.* **1969**, *51*, 635−636.

(44) Ustinov, E. A.; Do, D. D.; Jaroniec, M. Application of density functional theory to equilibrium adsorption of argon and nitrogen on amorphous silica surface. *Appl. Surf. Sci.* **2005**, in press.

(45) Ustinov, E. A.; Do, D. D.; Jaroniec, M. Adsorption of argon and nitrogen in cylindrical pores of MCM-41 materials: Application of density functional theory. *Appl. Surf. Sci.* **2005,** in press.

(46) Ustinov, E. A.; Do, D. D.; Jaroniec, M. *J. Phys. Chem. B* **2005**, *109*, 1947−1958.

(47) Weeks, J. D.; Chandler, D.; Andersen, H. C. *J. Chem. Phys.* **1971**, *54*, 5237−5247.

(48) Madden, W. G. *J. Chem. Phys.* **1992**, *96*, 5422−5432.

(49) Given, J. A. *J. Chem. Phys.* **1995**, *102*, 2934−2945.

(50) Neimark, A. V.; Ravikovitch, P. I.; Grün, M.; Schüth, F.; Unger, K. K. *J. Colloid Interface Sci.* **1998**, *207*, 159−169.

(51) Jaroniec, M.; Kruk, M.; Olivier, J. P. *Langmuir* **1999**, *15*, 5410−5413.

(52) Tikhonov, A. N. *Dokl. AN SSSR* **1943**, *39*, 195−198.

(53) Tikhonov, A. N. *Dokl. AN SSSR* **1963**, *153*, 49−52.

(54) Ustinov, E. A.; Do, D. D. *Langmuir* **2003**, *19*, 8349−8357.

(55) Ustinov, E. A.; Do, D. D. *Langmuir* **2004**, *20*, 3791−3797.

(56) Matos, J. R.; Mecuri, L. P.; Kruk, M.; Jaroniec, M. *Chem. Mater.* **2001**, *13*, 1726−1731.

CT049903Z